Kinetostatic analysis of a class of planar 2-DOF tensegrity manipulators

Antoine Lenoir, Christine Chevallereau, Alexandre Pitti, Philippe Wenger

Kinetostatic analysis of a class of planar 2-DOF tensegrity manipulators

Antoine Lenoir[1], Christine Chevallereau[1], Alexandre Pitti[2], and Philippe Wenger[1]

[1] Nantes Université, ECN, CNRS, LS2N, Nantes, France {{Antoine.Lenoir, Christine.Chevallereau, Philippe.Wenger}@ls2n.fr}
[2] ETIS, Evry, France {alexandre.pitti@cyu.fr}

Abstract. This study focuses on a class of planar tensegrity manipulators consisting of two triangular platforms facing each other and linked by cables at their vertices. The two lateral cables are active, while the central cable is passive. The geometric and static workspaces are determined by their boundaries using algebraic calculations. We demonstrate that some of these manipulators exhibit two distinct workspace types associated with two different behaviors: (1) a two-dimensional workspace in the lower part similar to a two-degree-of-freedom (DOF) suspended cable robot, and (2) a nearly one-dimensional workspace in the upper part that enables stiffness modulation without substantial displacement, a behavior close to an antagonistically actuated one-DOF tensegrity joint with adjustable stiffness.

Keywords: Tensegrity, variable stiffness, static workspace

1 Introduction

Tensegrity manipulators are an interesting design choice thanks to their high strength-to-weight ratio and variable stiffness properties [1]. Such manipulators are often remotely actuated by motors placed on the base, with cables as transmission elements [2], [3]. An important measure to quantify the performance of manipulators is their workspace. Since tensegrity manipulators are driven by taut cables, their workspace is defined by the conditions of static equilibrium that can be achieved with positive cable forces [4], [5]. This study focuses on a class of planar tensegrity manipulators consisting of two triangular platforms facing each other and linked by cables at their vertices. The two lateral cables are active, while the central cable length is fixed. Therefore, these manipulators have two degrees of freedom (DOF). The geometric and static workspaces are determined by their boundaries using algebraic calculations. We show that these manipulators may exhibit a narrow region in their static workspace in which they behave like antagonistically actuated one-DOF tensegrity joints with tunable stiffness. The rest of this paper is organized as follows: Section 2 describes the manipulators under study. Section 3 studies their singularities. Section 4 defines their workspace and static workspace. Section 5 studies a subclass of manipulators that are candidates to variable stiffness. Finally, Section 6 concludes this work.

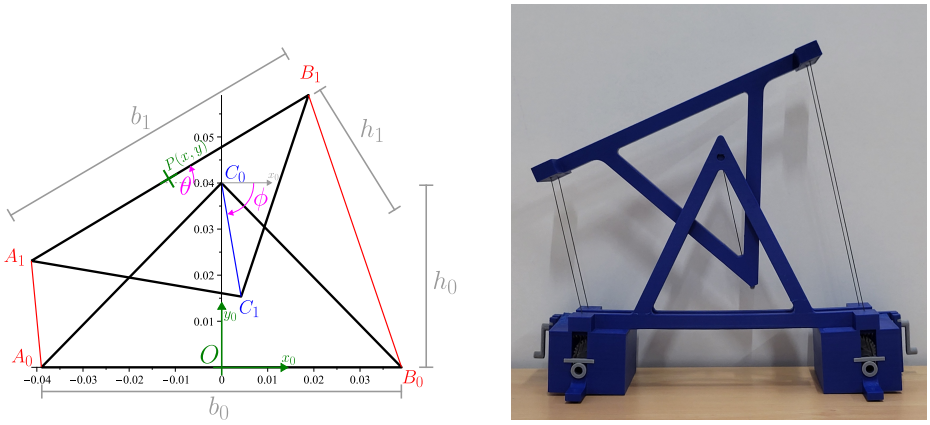

(a) (b)

Fig. 1: 1a : Schematic of a planar 2-DOF tensegrity manipulator driven by two active cables (in red). The length of the central cable (in blue) is fixed. 1b : Plastic model where a moving triangle is guided by two vertical triangular frames that are actuated by two pairs of parallel cables.

2 Manipulator description

Figure 1a shows an example of the tensegrity manipulators under study. It consists of two isosceles triangular platforms that face each other and are linked by cables at their vertices. The two lateral cables are active, whereas the central cable is passive. It is assumed that the manipulator is in a vertical plane and is therefore subject to gravity. It is assumed that the central cable is inelastic. In practice, it is made of steel, which has limited elasticity. The output point $\boldsymbol{P}$ is defined as the midpoint of the moving triangle base. Let A_i, B_i, C_i, $i = 0, 1$ denote the vertices of the base and moving triangles. A reference frame is attached to the base of the fixed triangle with the origin located at the base midpoint and the x-axis pointing to B_0. Let b_0 and h_0 (resp. b_1 and h_1) denote the base length and altitude of the fixed (resp. mobile) triangle, respectively. The length of the central cable is denoted by l_0. In Fig. 1a, $b_0 = 0.078$ m, $b_1 = 0.070$ m, $h_0 = 0.040$ m, $h_1 = 0.030$ m and $l_0 = 0.025$ m. Since the manipulator has only two DOFs, two parameters are enough to define its configuration. We choose the two angles θ and ϕ, defined as the moving platform orientation and the angle of the central cable, respectively. These angles are both measured counterclockwise with respect to the x-axis. The Cartesian coordinates (x,y) of $\boldsymbol{P}$ are given by :

$$\begin{cases} x = l_0 c\phi - h_1 s\theta \\ y = h_0 + l_0 s\phi + h_1 c\theta \end{cases} \tag{1}$$

where $s\theta = \sin(\theta)$, $s\phi = \sin(\phi)$, $c\theta = \cos(\theta)$, $c\phi = \cos(\phi)$.

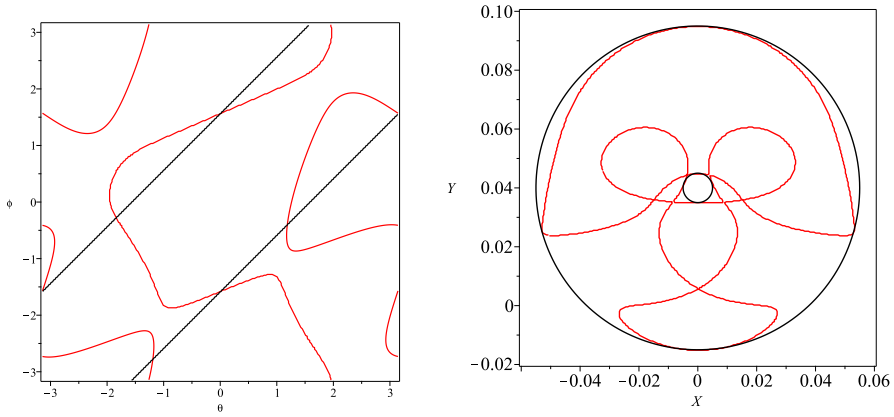

(a) (b)

Fig. 2: Singularity plot in (θ, ϕ) Fig. 2a_1 and in (x, y) Fig. 2b, for the manipulator of Fig. 1a. Parallel and serial singularities are represented in red and black respectively.

Next, we identify the singularities of the manipulator. We will show that they contribute to the boundaries of the static workspace.

3 Singularity analysis

A parallel singularity occurs wherever the lines of the three cables intersect, as in a 3-RPR parallel manipulator [7]. The intersection condition of the 3 cable lines can be written as:

$$\begin{aligned} &4l_0 s\theta \left(h_1 b_0 + b_1 h_0\right)\left(c^2\phi\right) + \left(-b_0\left(b_1^2 + 4h_1^2\right)\left(c^2\theta\right)\right. \\ &\left. - 4\left(h_0 + l_0 s\phi\right)\left(h_1 b_0 + b_1 h_0\right) c\theta + b_0\, b_1^2 - 4b_1 h_0 h_1\right) c\phi \\ &+ \left(-\sin\phi\left(b_1^2 + 4h_1^2\right) c\theta + \left(b_1 b_0 - 4h_1 h_0\right) s\phi - 4l_0 h_1\right) b_0 s\theta = 0 \end{aligned} \tag{2}$$

Unlike in a classical 3-RPR parallel manipulator, the central cable in our case has a fixed length, which creates additional singularities. These are serial singularities that occur when C_0, C_1 and P are aligned, i.e. $\phi = \theta \pm \pi/2$. In such configurations, no velocity can be produced in the C_0C_1P direction.

Figure 2a shows the plot of the parallel (in red) and serial (in black) singularities in the plane (θ, ϕ) for the manipulator of Fig. 1a.

We now determine the singularities in the workspace. The serial singularities are defined here by 2 circles centered at C_0 and of radii $|l_0 - h_1|$ and $l_0 + h_1$, respectively. They determine the external and internal workspace boundaries. The expression of the parallel singularities as functions of x and y can be obtained

upon eliminating θ and ϕ from Eq. (1) and Eq. (2). This is achieved using the tan-half angle substitution to make all equations algebraic. We then use the *Siropa* library of Maple™ for all eliminations [6]. The resulting equation is a very large 10th-degree polynomial in x and y. It is not reported here due to lack of space. Fig. 2b shows the singularity plot in (x, y) for the manipulator of Fig. 1a.

When the two triangles are congruent (i.e. of same dimensions, as the design analyzed in section 5), the expression of the parallel singularities is much simpler. In fact, Eq. (2) factors and one of the factors is associated with the particular case where the cable lines are parallel. Note that for non-congruent triangles, the three cables can be parallel only when the two active cables align with the x-axis. Using simple geometric arguments, this condition can be written as $\phi = \theta/2 \pm \pi/2$. The associated condition in the Cartesian space results in an equation of degree 4 in x and y ($h = h_0 = h_1$ and $b = b_0 = b_1$):

$$y^4 - 4y^3h + \left(4h^2 - l_0^2 + 2x^2\right) y^2 - 4x^2yh + x^4 - x^2l_0^2 = 0 \tag{3}$$

The second factor is a 6^{th} degree polynomial:

$$\begin{aligned}
&\left(-256l_0^2 + 256y^2\right) h^8 - 256y\left(-3l_0^2 + x^2 + 3y^2\right) h^7 \\
&+ \left(960y^4 + \left(128b^2 - 1088l_0^2 + 512x^2\right) y^2 - 128b^2l_0^2 + 64x^4 + 64x^2l_0^2 + 128l_0^4\right) h^6 \\
&- 64\left(9y^4 + \left(5b^2 - 12l_0^2 + 10x^2\right) y^2 + \left(-5l_0^2 + x^2\right) b^2 + x^4 - 4x^2l_0^2 + 3l_0^4\right) y\, h^5 \\
&+ \Big(144y^6 + \left(320b^2 - 240l_0^2 + 304x^2\right) y^4 \\
&+ \left(16b^4 + \left(-384l_0^2 + 160x^2\right) b^2 + 176x^4 - 224x^2l_0^2 + 112l_0^4\right) y^2 \\
&+ 16\left(x - l_0\right)\left(x + l_0\right)\left(b^4 + \left(-4l_0^2 - 2x^2\right) b^2 + \left(l_0^2 + x^2\right)^2\right)\Big) h^4 - 32\left(b^2 + x^2/2\right. \\
&\left.+ 9y^2/2 - 5l_0^2/2\right) b^2y\left(-l_0^2 + x^2 + y^2\right) h^3 + 8b^2\left(-l_0^2 + x^2 + y^2\right)\left(3y^4 + \left(3b^2 - 4l_0^2 + 2x^2\right) y^2\right. \\
&\left.+ \left(-l_0^2 + x^2\right) b^2 - x^4 + l_0^4\right) h^2 - 8b^4y\left(-l_0^2 + x^2 + y^2\right)^2 h + b^4\left(-l_0^2 + x^2 + y^2\right)^3
\end{aligned} \tag{4}$$

4 Static analysis

As the manipulators' legs are cables, the cable tensions should remain within their minimum and maximum limits in every equilibrium configuration. The equilibrium equations of the moving platform can be written as follows:

$$\mathbf{W}_1(\phi, \theta)\mathbf{t} + \mathbf{w}_p(\phi, \theta) = \mathbf{0}_3 \tag{5}$$

where $\mathbf{0}_3$ is the 3-dimensional zero vector, $\mathbf{w}_p$ is the gravity wrench, $\mathbf{t}$ is the cable tension vector and $\mathbf{W}_1$ is the wrench matrix [10].

The boundaries of the static workspace are defined by the tension limits $\underline{t_i}$ and $\overline{t_i}$. Their equations are obtained by setting one of the three cable tensions t_i to its limit. One of the two remaining tensions, t_j (where $j \neq i$), is solved for using one of the static equations, and the result is reported in another static equation. Note that the specific choice of equation does not matter, as it does not affect the result. In the resulting equation, the final tension, t_k, where $k \neq i$

and $k \neq j$, appears as a factor and can be eliminated. Finally, the curves defined by the bounding equations, $t_i = \underline{t_i}$ and $t_i = \overline{t_i}$ for $i = 0, 1, 2$, and by the singularities, create a set of regions. However, not all of these regions are valid, as each bounding equation $t_i = \underline{t_i}$ and $t_i = \overline{t_i}$ must satisfy $\underline{t_j} \leq t_j \leq \overline{t_j}, j \neq i$. In practice, the regions belonging to the static workspace can be identified by selecting an arbitrary point within each cell, and then testing the tension limits.

Figure 3a shows the resulting static workspace (the green areas) in the (θ, ϕ) plane. It also shows the plots of the parallel singularities (in red) and the boundaries for a moving platform with a mass of 0.05 kg and minimal tension bounds chosen as zero. For the sake of clarity, the serial singularity plots have been omitted. The curves $t_0 = 0$ (resp. $t_1 = 0$, $t_2 = 0$) associated with the central (resp. left and right) cable are depicted in blue dotted lines (resp. in cyan and blue solid lines). We observed that the curves $t_0 = \overline{t_0}$, $t_1 = \overline{t_1}$, $t_2 = \overline{t_2}$ (not shown for the sake of clarity) are very close to the singularity curves even when $\overline{t_i}$ is not very large (100 N for the manipulator at hand).

To obtain the static workspace plot in the Cartesian space, the bounding equations $t_i = \underline{t_i}$ and $t_i = \overline{t_i}$ must be written as functions of x and y. This can be achieved by following the same process as for the equations of the parallel singularities. Figure 3b shows the plots of all boundaries in the Cartesian space. The static workspace is shown in green. As before, the boundaries associated with the maximal tensions $\overline{t_i} = 100$ N are almost coincident with the parallel singularity curves. Note that, in the same way as the serial singularities, the parallel singularities also contribute to the boundaries of the static workspace. This is generally not the case for fully-parallel manipulators.

To improve appreciation of the static workspace and as a means of double-checking, we generated it numerically by scanning θ and ϕ (Fig. 4).

5 Tensegrity manipulator with stiffness modulation

From Fig. 3a and 3b, it appears that the static workspace comprises one large region — bearing in mind that the opposite sides of Fig. 3a must be joined — and two narrow regions that converge at a single point in the center. This single point corresponds to a configuration in which $\theta = 0$ and $\phi = -\pi/2$, which is singular since all cables are vertical. In this configuration, the tensions can be adjusted according to a desired stiffness, provided that $t_1 = t_2 = t_0/2 - mg/2$. Outside this point, a change in the cable tensions will slightly modify the manipulator configuration within the narrow region and modify it more significantly within the large region. The geometric parameters can be selected based on the expected performance of the manipulator. The design shown in Fig. 1a has a rather large workspace in its bottom area. On the other hand, a narrow workspace can be an interesting choice for collaborative tasks where stiffness can be controlled. Let us select a design with *congruent* triangles defined by $b_0 = b_1$=0.080 m, $h_0 = h_1$=0.060 m, and l_0=0.010 m, the static workspace of which is shown in Fig. 5. In the upper, narrow region, the manipulator's behavior resembles that of an antagonistically actuated anti-parallelogram joint with stiffness variation [8],

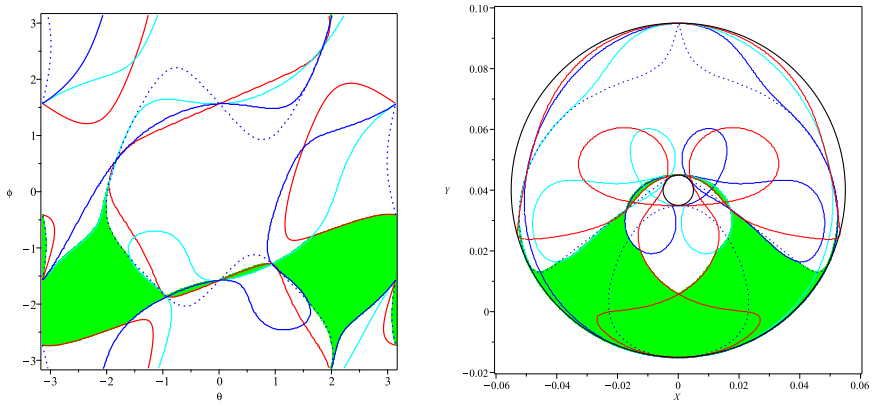

(a) (b)

Fig. 3: Singularities and tension limits in (θ, ϕ), Fig. 3a, and in (x, y), Fig. 3b. The green areas show the static workspace. The red curves are parallel singularities. The dotted blue curve (resp. the solid cyan and solid blue curves) corresponds to a zero tension in the central (resp. the left and right) cable.

[9]. In practice, if both forces are increased by the same amount starting from a given configuration, the manipulator stiffness may increase while its configuration remains almost unchanged. To verify this hypothesis, we have calculated the stiffness matrix and its eigenvalues and eigenvectors. The stiffness matrix was calculated using the second derivatives of the joint's potential energy with respect to x, y, and . The potential energy accounts for gravity and cable linear elasticity. The two lateral cables are made of nylon (stiffness k_c = 7735 N/m) while the central cable is made of steel (stiffness k = 1.26 10^6 N/m). The following two sets of actuation forces are applied to the moving triangle: (20 N, 10 N) and (100 N, 50 N), i.e. the second set of forces are five times greater than the first. We assume the cable free lengths are kept constant by a perfect control law. The corresponding positions (shown in Fig. 5) are very close: (x = 0.02263 m, y = 0.10486 m) and (x = 0.02309 m, y = 0.10454 m). The corresponding eigenvalues of the stiffness matrix are (k_1 = 1.27567 10^6 N/m, k_2=3323 N/m, k_3=25 N/m) and (k_1 = 1.27567 10^6 N/m, k_2=16279 N/m, k_3=21 N/m). The first eigenvalue is associated with the stiffness along the central cable direction and remains almost unchanged, close to that of the steel cable. The second eigenvalue is associated with the stiffness along a direction perpendicular to the central cable and is almost multiplied by 5. The last eigenvalue, the rotational stiffness, decreases slightly. With this behavior, the design can be used as a tensegrity joint for the purpose of designing lightweight robots that are suitable for physical interactions. Compared to the anti-parallelogram joint used in [8] and [9], the proposed design is simpler because it does not include any revolute joints. Furthermore, it can accommodate 2-DOF motions if required.

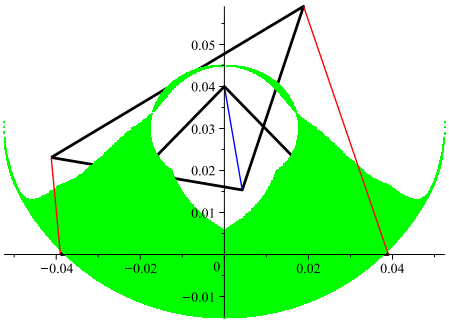

Fig. 4: Static workspace obtained by scanning.

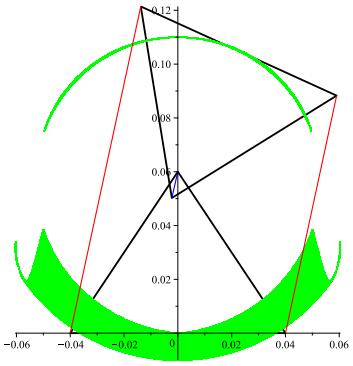

Fig. 5: A tensegrity manipulator with stiffness tuning.

6 Conclusions

This paper investigated the geometric and static workspaces of a class of planar, 2-DOF tensegrity manipulators composed of two triangles. These triangles face each other and are connected by two lateral active cables and one central fixed-length cable. The equations of the serial and parallel singularities were determined using algebraic tools. The static workspace was characterized using a static model, taking into account positive and bounded cable forces. We showed that parallel singularities can be employed to delineate certain boundaries within the static workspace. The analysis revealed that, for certain choices of geometric parameters, the static workspace contains a narrow region in its upper part, in which the manipulator behaves similarly to an antagonistically actuated one-DOF tensegrity joint. In this region, variations in the actuation forces primarily affect the stiffness of the manipulator while causing only minor changes to its

position. Like a suspended cable robot, the static workspace is wider at the bottom. A stiffness analysis with elastic cable models confirmed the existence of a significant stiffness modulation capability. Specifically, increasing the antagonistic cable tensions resulted in a significant increase in stiffness perpendicular to the central cable, while maintaining the end-effector position. This behavior makes this class of manipulators especially suitable for applications involving physical human–robot interaction and collaborative robotics, where lightweight structures and tunable compliance are desirable.

The ongoing work aims to further investigate how manipulator geometry influences the size and structure of the static workspace and its stiffness modulation capabilities. Then, experiments will be conducted on a prototype to verify the theoretical results. We are also working on extending this research to 3D joint models, as discussed in [11].

7 Acknowledgments

This work was supported by the French National Research Agency (ANR) under the France 2030 program, as part of the PEPR O2R–AS1 project (grant number ANR-22-EXOD-0005).

References

1. Y. Liu, Q. Bi, X. Yue, J. Wu, B. Yang, Y. Li, A review on tensegrity structures-based robots, Mech. and Mach. Theory 168 (2022) 104571.
2. X. Yue, Xu Yin, Z. Sun, L. Liu, Y. Wang, G. Xu, C. Cao, L. Zhang, Flexible, lightweight, tunable robotic arms enabled by X-tensegrity inspired structures, Composite Structures 344 (2024) 0263–8223
3. F. Li, H. Peng, H. Yang, Z. Kan, A symplectic kinodynamic planning method for cable-driven tensegrity manipulators in a dynamic environment, Nonlinear Dynamics 106 (2021) 2919–2941.
4. Q. Boehler, I. Charpentier, M. S. Vedrines, P. Renaud, Definition and computation of tensegrity mechanism workspace, Journal of Mech. and Rob. 7 (4) (2015) 044502.
5. M. Arsenault, C. M. Gosselin, Kinematic, static and dynamic analysis of a planar 2-DOF tensegrity mechanism, Mech. and Mach. Theory 41 (9) (2006) 1072–1089.
6. Chablat, D., Moroz, G., Rouillier, F., Wenger, P.: Using maple to analyse parallel robots. In: Gerhard, J., Kotsireas, I. (eds.) Maple in Mathematics Education and Research. pp. 50–64. Springer International Publishing, Cham (2020)
7. Zein M, Wenger P, Chablat D. Singular curves in the joint space and cusp points of 3–RPR parallel manipulators. Robotica. 2007;25(6):717–724.
8. M. Furet, P. Wenger, Kinetostatic analysis and actuation strategy of a planar tensegrity 2-X manipulator, Journal of Mech. and Rob. 11 (6) (2019) 060904.
9. Muralidharan, V., Wenger, P.: Optimal design and comparative study of two antagonistically actuated tensegrity joints. Mech. Mach. Theory **159**, 104249 (2021).
10. Christine Chevallereau, Philippe Wenger, Stéphane Caro: Compound Cable-driven Parallel Robot for Improved Wrench-feasible Workspace, In: Lenarčič, L., Husty, M. (eds.) ARK 2024. pp. 130–139. Springer Proc. in Advance Rob. (2024)
11. Y. Hao, X. Wang, X. Song, Y. Li, H. Fu, A.Pui-Wai Lee, K. Cheung, J. Lam, K. Kwok: A Tensegrity Joint for Low-Inertia, Compact, and Compliant Soft Manipulators, Advanced intelligent systems, 6, 2300079, (2024)